Zeitschrift: Helvetica Physica Acta
Band: 43 (1970)
Heft: 8

Artikel: Dynamic nuclear polarization in ruby
Autor: Niebuhr, H.H. / Hundt, E.E. / Brun, E.
DOI: https://doi.org/10.5169/seals-114192

Dynamic Nuclear Polarization in Ruby[1])

by **H. H. Niebuhr**[2]), **E. E. Hundt** and **E. Brun**

Physik-Institut der Universität Zürich, 8001 Zürich, Switzerland

(21. V. 70)

Abstract. The solid-state effect has been investigated in synthetic ruby ($Al_2O_3:Cr^{3+}$) at both liquid helium and liquid nitrogen temperatures. At 1.55 °K an ^{27}Al nuclear polarization of 17% has been reached in a magnetic field of 11 kilogauss. Experiments have been performed which prove the existence of a spin temperature for the ^{27}Al spin system also under dynamic polarization conditions. At the lowest obtained spin temperature of 0.004 °K the sign of the quadrupole coupling constant e^2qQ for ^{27}Al has been determined to be positive. The sign has been derived from the intensity ratios of polarized and thermal equilibrium NMR signals. Unusual NMR line shapes have been found when microwave power is supplied to the sample at the center of an ESR line. This new polarization effect is related to the line broadening mechanisms in ruby. The ordinary polarization curves are compared with results from the slightly modified spin temperature theory of dynamic nuclear polarization as developed by Borghini.

I. Introduction

The solid-state effect [1–4] is a well known method to dynamically polarize nuclear spin systems, where simultaneous transitions of paramagnetic impurities and nuclear spins in a diamagnetic solid are induced by a microwave field. It has been investigated previously in a large number of substances mainly with electronic and nuclear spins 1/2 in order to achieve high spin polarizations and to study the dynamics of the phenomenon. With the present investigation we try to demonstrate its further application to problems where nuclear quadrupole effects are of importance. As a material synthetic ruby ($Al_2O_3:Cr^{3+}$) was chosen, because crystals of high quality are readily available, and which has been studied by various magnetic resonance techniques in great detail [5–11]. In our experiments enhancements of the ^{27}Al nuclear polarization as high as 120 at 77 °K and 360 at 1.55 °K are reached. A direct determination of the sign of the quadrupole coupling constant e^2qQ is possible by measuring the relative intensities of the ^{27}Al NMR lines at the low nuclear spin temperature of 0.004 °K achieved by dynamic polarization. When a Cr^{3+} ESR line is saturated near its center, unusual ^{27}Al NMR line shapes result. With this new effect ESR and NMR line broadening mechanisms can be studied at least in principle. It is found that the

[1]) Paper based upon a dissertation submitted to Universität Zürich by H. H. Niebuhr in partial fulfillment of the requirements for the Ph. D. degree. Research supported by the Schweizerischer Nationalfonds.

[2]) Present address: Department of Physics, Saint Louis University, Saint Louis, Missouri 63103, USA.

nuclear spin system is always in thermal equilibrium also under dynamic polarization conditions. From the results it will become clear that such investigations can be extended to other structures, and thus may become an important tool in this kind of work.

II. Experimental Procedure and Results

1. *Experimental techniques*

The experimental results which we present have been obtained with a conventional dynamic polarization setup described elsewhere [12]. It consists of a Varian V-3400 magnet, a simple spectrometer driven with a K 3038 klystron for detection and saturation of ESR lines at frequencies from 30 to 35 GHz, and a Q-meter detector for the NMR measurements. The NMR coil is wound directly around the crystal which is placed in arectangular multimode cavity in a suitable cryostat. The maximum power incident to the cavity is approximately 100 mW. The polarization enhancement is determined from the enhancement of the NMR signal with respect to its thermal equilibrium value. Polarization and relaxation times are derived from the rate of change of the NMR signal intensity after switching on or off the microwave power. Typical errors of time constants and enhancements are estimated to be about 10%. In order to obtain undistorted NMR signals the resonance frequency of the Q-meter has to be equal to the NMR frequency. To observe a quadrupole split NMR spectrum it is advantageous to use a set of different NMR tank circuits, each properly tuned to one line. For the various measurements we had at our disposal 5 different capacitors which could be connected to the circuit with a switch.

2. *Samples*

The structure of corundum (α-Al_2O_3) offers some specific advantages for dynamic polarization experiments. Single crystals of excellent quality and doped with various paramagnetic impurities can be easily obtained. The cations occupy equivalent sites thus yielding a single quadrupole split ^{27}Al NMR spectrum [6]. Similarly, the ESR spectra of substitutionally embedded impurities [5, 13–18] are easy to interpret and both the NMR and ESR lines are fairly narrow.

Particularly high quality laser rubies (Al_2O_3: Cr^{3+}) with a low concentration of other than Cr^{3+} impurities are suitable for obtaining a high ^{27}Al spin polarization when microwave power is supplied to the crystal in the neighborhood of one of the Cr^{3+} ESR lines. Since it is difficult to predict the optimal Cr^{3+} concentration, a number of rubies with different chromium contents were investigated. The maximum nuclear polarization enhancement E_{max}, and the transverse nuclear spin relaxation time T_n, were measured as a function of the Cr^{3+} concentration at a temperature of about 1.9 °K and with 100 mW incident microwave power at 35 GHz. The angle ϑ between the static magnetic field H_0 and the crystal c-axis was approximately 50°. The results shown in Figure 1 indicate a correlation between E_{max} and T_n[3]). In rubies with more than 0.05% Cr^{3+} E_{max} and T_n fall off strongly, which might be due to the formation

[3]) The chromium concentrations (at. wt. %) given by the manufacturer and listed in Fig. 1 are somewhat uncertain. Hence the crystal with nominal 0.05% probably contains less Cr^{3+}.

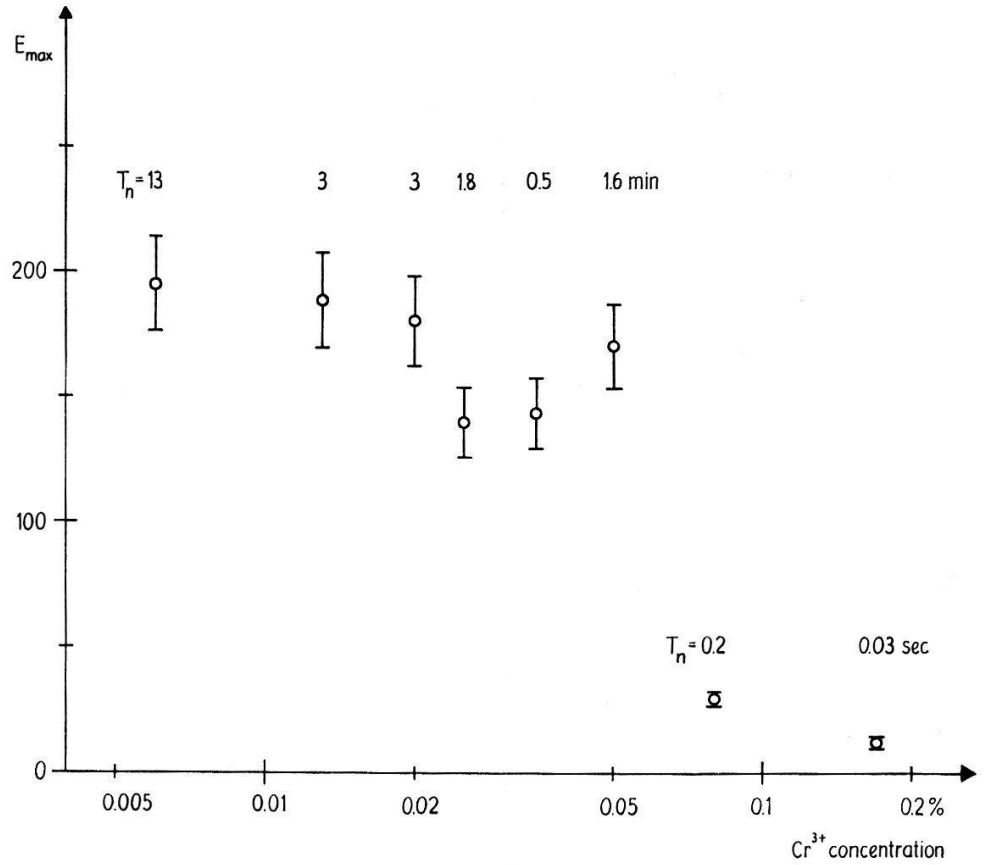

Figure 1
Maximum measured enhancements E_{max} and nuclear relaxation times T_n at 1.9°K.

of rapidly relaxing chromium pairs and triads [19–21]. Typical widths of the polarization curves, as measured between points of maximum positive and negative enhancement, are 50–130 gauss.

Based on these results, rubies with Cr^{3+} concentrations ranging from 0.006% to 0.025% were chosen for the more detailed measurements.

3. *Electron spin resonance of* Cr^{3+}

Cr^{3+} in ruby has an effective electron spin of 3/2 in its lowest states. The Hamiltonian is [5]

$$\mathcal{H} = g_{\parallel}\,\beta\,H_z\,S_z + g_{\perp}\,\beta(H_x\,S_x + H_y\,S_y) + D\left[S_z^2 - \frac{1}{3}\,S\,(S+1)\right] \tag{1}$$

with the z-direction parallel to the crystal c-axis.

$$g_{\parallel} = 1.9840 \pm 0.0006, \quad g_{\perp} = 1.9867 \pm 0.0006 \text{ and } D = -(5.747 \pm 0.003)\ \text{GHz}.$$

Using a standard diagonalization technique, the resonance magnetic field H_e as a function of the angle ϑ between the field and the c-axis has been computed for the various transitions at a fixed microwave frequency of 32.5 GHz. The results are shown in Figure 2. The hyperfine interaction of the Cr^{3+} ions with neighboring nuclei and lattice imperfections cause an inhomogeneous broadening of the ESR lines [22–24]. They can be built up from spin packets [25] whose amplitudes approximately show a Gaussian distribution $g\,(H_e - H_e')$. H_e' is the resonance field of such a packet and H_e

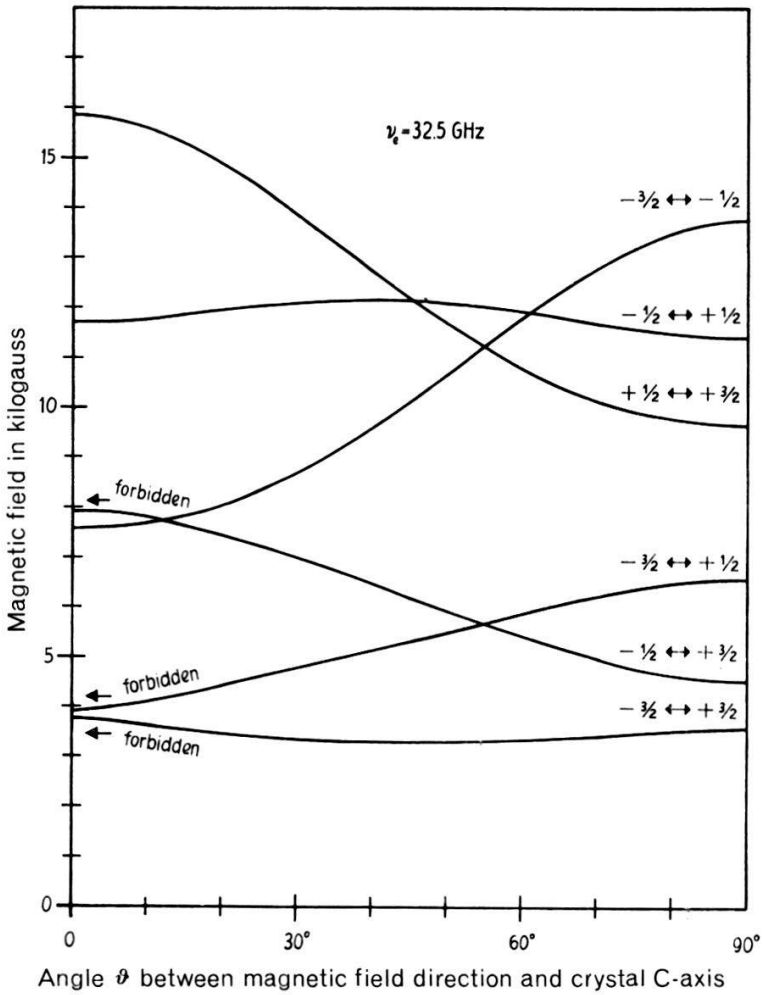

Figure 2
Resonance fields of Cr^{3+} in ruby.

the average resonance field of the total line. The line width of a single packet is caused by the spin-spin interactions of the paramagnetic ions and its line shape $k\,(H'_e - H)$ is approximately Lorentzian. Thus the shape of the resulting ESR line is

$$f(H) = \int_{-\infty}^{\infty} g\,(H_e - H'_e)\,k\,(H'_e - H)\,dH'_e\,. \tag{2}$$

In order to estimate the line width of a single packet, a numerically integrated ESR line has been fitted with $f(H)$ of equation (2). The half width at half maximum of $k\,(H'_e - H)$ was chosen as 2.75 gauss and the peak-to-peak width of the derivative of $g\,(H_e - H'_e)$ as 16.6 gauss. The result is shown in Figure 3 where it can be compared with similar fits of a Gaussian and a Lorentzian shape function. The accuracy is limited by the errors in determining the ESR line shape and by the small width of a spin packet line relative to the Gaussian envelope.

4. *Nuclear magnetic resonance of* ^{27}Al

^{27}Al in ruby occupies a site of point symmetry C_3. The electric nuclear quadrupole moment eQ of ^{27}Al interacts with the inhomogeneous local electric field. The field gradient tensor at the nuclear position is completely determined by the quadrupole coupling constant e^2qQ, since this tensor has rotational symmetry about the z

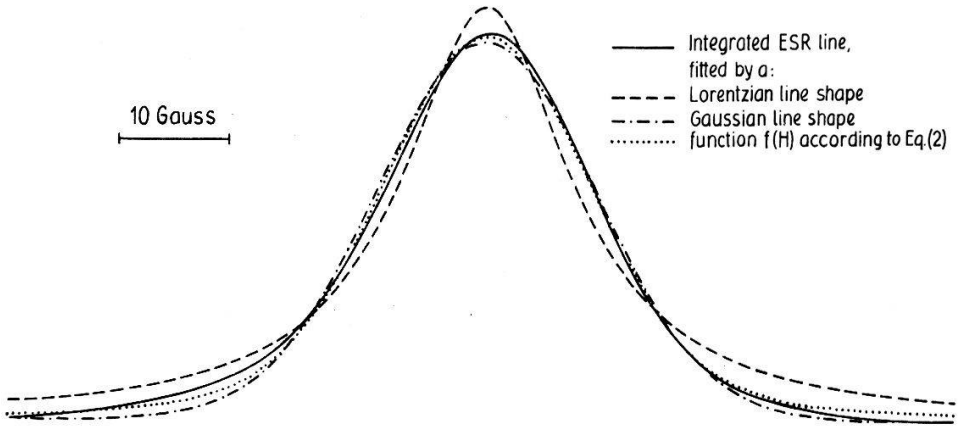

Figure 3
ESR line for $-3/2 \leftrightarrow -1/2$ transition. $T = 77\,°\mathrm{K}$, $\vartheta \approx 0°$, 0.025% Cr^{3+} in ruby.

principal axis. The quantity eq is the negative derivative of the field strength in the direction of the z axis. The nuclear spin Hamiltonian is [26]

$$\mathcal{H} = -\gamma_n \hbar \boldsymbol{H} \boldsymbol{I} + \frac{e^2 q Q}{4 I (2 I - 1)} [3 I_z^2 - I (I + 1)] , \tag{3}$$

where the z direction is parallel to the 3-fold crystal axis. The energy levels derived by standard first order perturbation theory are

$$E_m = -\gamma_n \hbar H_0 m + \frac{e^2 q Q}{8 I (2 I - 1)} (3 \cos^2\vartheta - 1) [3 m^2 - I (I + 1)] \tag{4}$$

$\gamma_n = 2\pi \times 1.1094$ MHz/kG is the gyromagnetic ratio, $I = 5/2$ the spin, and m the magnetic quantum number of ^{27}Al. ϑ is the angle between the 3-fold axis and the static magnetic field H_0. In this approximation the NMR spectrum consists of five equally spaced lines: the central line and two pairs of satellites of corresponding transitions $m \leftrightarrow m - 1$ and $-m + 1 \leftrightarrow -m$. If H_0 is applied parallel to the c-axis of the crystal, the ^{27}Al NMR lines show a partly resolved structure due to the dipole interaction of nearest ^{27}Al neighbors. From the line structure the sign of e^2qQ has been derived by Silver, Kushida and Lambe [27].

5. *^{27}Al nuclear polarization*

The dynamic polarization of ^{27}Al in ruby has been investigated previously by various authors [28–30]. The reported enhancements of the ^{27}Al spin polarization are 30 at 4.2 °K, 44 at 77 °K, and 6 at room temperature.

We have observed an enhancement which is 120 at 77 °K and 360 at 1.55 °K. The latter corresponds to a nuclear polarization of 17.3%. It has been reached when microwave power was supplied in the neighborhood of two crossing Cr^{3+} ESR transitions. At 77 °K the polarization curve has approximately the width and line shape of the derivative of the unsaturated ESR absorption line, thus indicating the differential solid-state effect. At the temperature of liquid helium the polarization curve is considerably wider. Figure 4 shows the enhancement as a function of magnetic field and microwave power at 4.2 °K. In all cases where it has been examined, $E - 1$

is an antisymmetric function of $\Delta H = H_0 - H_e$ within experimental error (Fig. 5). E denotes the enhancement of the ^{27}Al NMR signal with respect to the thermal equilibrium value and H_e is the ESR field.

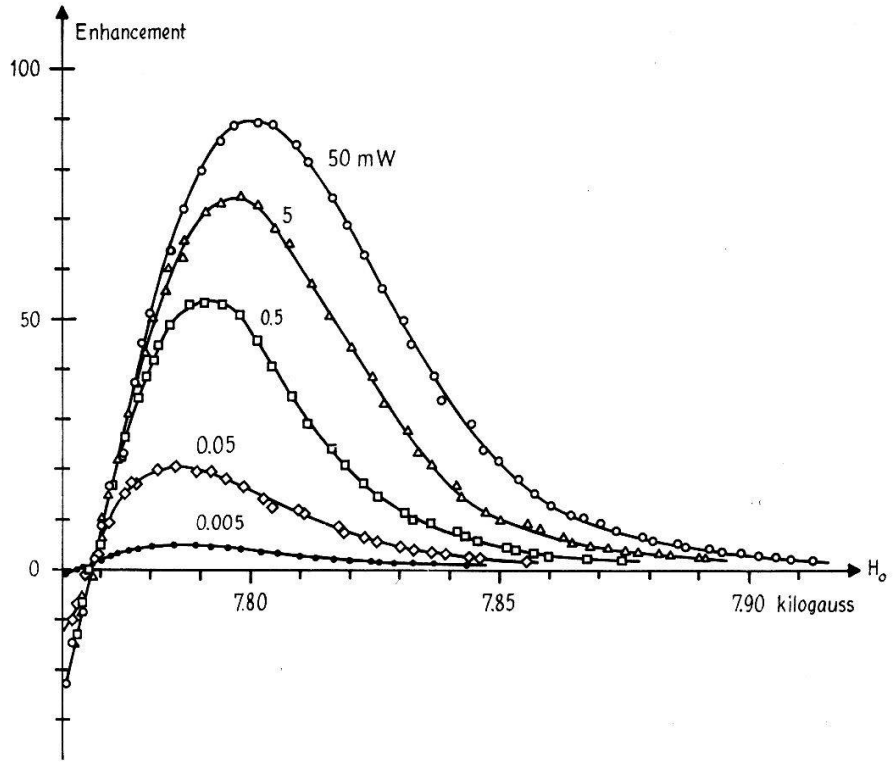

Figure 4
Polarization curves for various microwave powers. $T = 4.2°K$, $\vartheta \approx 0°$, 0.025% Cr^{3+} in ruby.

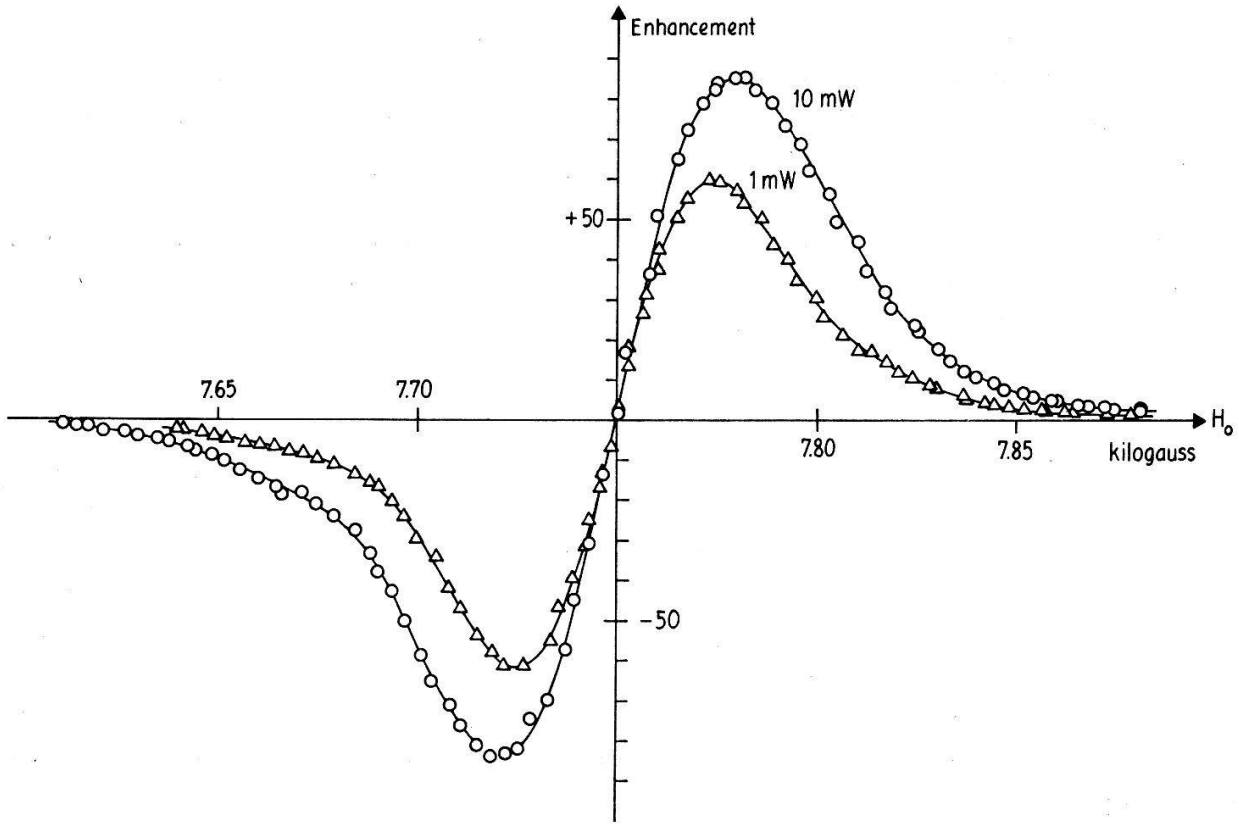

Figure 5
Polarization curves at 10 mW and 1 mW microwave power. $T = 4.2°K$, $\vartheta \approx 0°$, 0.025% Cr^{3+} in ruby.

6. *Determination of the sign of the quadrupole coupling constant e^2qQ of* ^{27}Al

The absolute value of the quadrupole coupling constant e^2qQ is commonly derived from the observed NMR line splitting [6]. The sign, however, cannot be determined directly from the NMR intensities at ordinary temperatures as Abragam [31] has shown. If the spin temperature is lowered to the order of a few milli-degrees absolute, intensity differences of corresponding satellites are expected which make possible the determination of the sign of the quadrupole coupling constant. This method has been demonstrated by Abragam and Chapellier for the coupling constant of ^{139}La in lanthanum magnesium nitrate [32].

For ^{27}Al with $I = 5/2$ and a positive gyromagnetic ratio γ_n [33], the populations for the different spin states and the relative intensities of the NMR transitions are listed in Table 1. Usually the linear terms in the expansion of the Boltzmann functions have to be retained only and all the signal intensities change linearly with $\delta = h\nu_n/kT$. Corresponding satellites thus have the same intensity. At low enough temperatures the quadratic terms cannot be neglected. They give rise to different intensities for the corresponding lines. NMR transitions between lower and higher spin levels become distinguishable. Thus the sign of e^2qQ can easily be determined with the aid of equation (4). In order to have quadratic terms in δ which are 5% of the linear ones, the spin temperature has to be 0.013 °K in a magnetic field of 12 kilogauss. Since an ^{27}Al spin temperature of this order of magnitude is easily attainable, as can be seen from the polarization experiments described above, two different experiments have been performed to determine the sign of e^2qQ of ^{27}Al in Al_2O_3.

1. A ruby containing 0.013% Cr^{3+} was mounted in the microwave cavity of our polarization setup such that the angle ϑ between the c-axis and the magnetic field was about 50°. The crystal was irradiated with the highest possible microwave power in the neighborhood of the $-3/2 \leftrightarrow -1/2$ Cr^{3+} ESR transition, which is very sensitive to a change in ϑ (Fig. 2). The angle ϑ was consecutively set to two different values in order to obtain optimal positive and negative polarization without changing the magnetic field strength. The NMR signals have been recorded for the two settings such that the intensities of corresponding polarized satellites can be compared. In going from a positive to a negative enhancement the corresponding satellites vary in intensity as is expected from a positive value of e^2qQ. However, the observed effects are rather small because the frequencies of the NMR lines change with ϑ thus introducing additional uncertainties.

2. To improve the sensitivity the angle ϑ was set to approximately 61°, where the $-3/2 \leftrightarrow -1/2$ and the $-1/2 \leftrightarrow +1/2$ ESR transitions coincide (Fig. 2). An enhancement of 360 was reached, which is twice as large as in the first experiment. With all the instrumental parameters kept constant the enhanced signals and those at thermal equilibrium without microwave power present have been carefully recorded. Typical results are shown in Figure 6. The thermal equilibrium (Fig. 6a) and the polarized NMR signals (Fig. 6b) show distinct differences in the intensity ratios of each particular line. Since the signals of Figure 6 were taken with a single Q-meter tank circuit tuned to a fixed frequency, the outer lines are slightly asymmetric. Therefore, only signal ratios of identical satellites should be compared. The enhancement of the five NMR lines grows with increasing frequency. For $\vartheta \approx 61°$ the factor $(3\cos^2\vartheta - 1)$

is negative. Therefore, the sign of the quadrupole coupling constant e^2qQ is positive [34]. The measured enhancements can be explained by a Boltzmann factor $\delta = 0.151$. This corresponds to a polarization $P = +17.3\%$ and a nuclear spin temperature of 4×10^{-3} °K with an estimated error of 10%. The values of δ and P and of the theoretical enhancements presented in Table 2 have been calculated using the full, properly normalized, exponential functions of Table 1.

Our determination of the sign of e^2qQ is in agreement with the result of Silver et al. [27]. These authors were able to determine the sign of e^2qQ in Al_2O_3 because of the dipolar structure of the NMR lines for $\vartheta \approx 0°$. Since such a structure is usually not present in other compounds and for other nuclei, the method of cooling the nuclear spin system with the aid of dynamic polarization is presumably the most promising one to measure the sign of further quadrupole coupling constants. However, its application is possible only when a considerable enhancement can be achieved at the temperature of liquid helium.

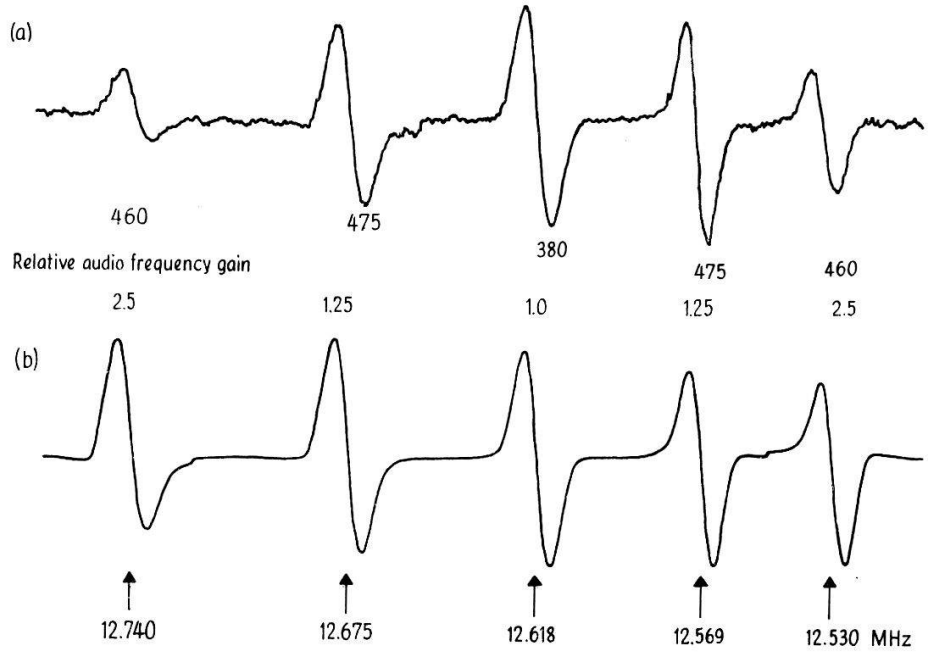

Figure 6
NMR of ^{27}Al in ruby (a) at thermal equilibrium and (b) enhanced by simultaneous saturation of both the $-3/2 \leftrightarrow -1/2$ and $-1/2 \leftrightarrow +1/2$ ESR transitions.

Table 1
Populations of nuclear levels and NMR intensities for nuclei with $I = 5/2$ and $\gamma_n > 0$ at thermal equilibrium. $\delta = h\nu_n/k\,T$.

Quantum number m	Population under positive polarization	Relative intensity of signal
$-5/2$	$e^{-5\delta}$	
$-3/2$	$e^{-4\delta}$	$\propto e^{-4\delta} - e^{-5\delta} = \delta - 9/2\,\delta^2 \pm \ldots$
$-1/2$	$e^{-3\delta}$	$\propto e^{-3\delta} - e^{-4\delta} = \delta - 7/2\,\delta^2 \pm \ldots$
$+1/2$	$e^{-2\delta}$	$\propto e^{-2\delta} - e^{-3\delta} = \delta - 5/2\,\delta^2 \pm \ldots$
$+3/2$	$e^{-\delta}$	$\propto e^{-\delta} - e^{-2\delta} = \delta - 3/2\,\delta^2 \pm \ldots$
$+5/2$	1	$\propto 1 - e^{-\delta} = \delta - 1/2\,\delta^2 \pm \ldots$

7. *Spin temperature, cross relaxation and polarization times of the ^{27}Al spin system*

The theoretical enhancements listed in Table 2 have been calculated under the assumption that the nuclear spin system under dynamic polarization conditions reaches an equilibrium state to which a spin temperature can be assigned. The agreement of theoretical and experimental enhancements clearly demonstrates the correctness of this assumption which is not a trivial one. This thermal equilibrium has been found in all our experiments, where it has been looked for.

Table 2
Experimental and theoretically calculated ($\delta = 0.151$) enhancements under simultaneous saturation of the $-3/2 \leftrightarrow -1/2$ and $-1/2 \leftrightarrow +1/2$ Cr^{3+} ESR transitions. Satellites *a* to *e* are the ^{27}Al NMR signals in the order of decreasing frequency.

Satellite	Experimental enhancement	Calculated enhancement
a	509	505
b	430	435
c	360	374
d	342	321
e	269	276

An experiment has been performed which gives additional support to the idea of the existence of a spin temperature under dynamic polarization. Sufficiently strong radiofrequency power was supplied to the sample which saturated a selected single ^{27}Al NMR line in less than one second. This caused the other ^{27}Al lines to decrease exponentially. In a ruby with 0.006% Cr^{3+} at $T = 2\,°K$ the characteristic time constant T^* was measured to be about 2 sec for $\vartheta \approx 60°$ and about 13 sec for $\vartheta \approx 0°$. Since T^* is much shorter than the polarization time T'_{np} for the same specimen, it becomes evident that it is the fast cross relaxation described by T^* which maintains the equilibrium at helium temperatures under dynamic polarization conditions. For the cross relaxation the electronic dipole-dipole energy $\mathcal{H}_{SS}$ acts as a reservoir which takes up the excess energy [35].

The change of the ^{27}Al nuclear polarization after switching on or off the microwave power can be described by an exponential function in all observed cases. The characteristic time constant T_1 is either the polarization time T'_{np} or the nuclear relaxation time T_n. In our experiments even at the lowest attainable temperatures and highest microwave powers T'_{np} is not much shorter than T_n. Figure 7 shows the measured values of T'_{np} for a microwave power of 50 mW in a ruby with 0.025% Cr^{3+} at $T = 1.85\,°K$ and $\vartheta \approx 0°$.

8. *^{27}Al NMR line shape under dynamic nuclear polarization*

According to the standard polarization theories [1, 3, 4] the enhanced NMR signals are expected to have the same line shape as the ones at thermal equilibrium without microwave power present. In the vicinity of the center of a homogeneously broadened ESR line a position should exist, where the polarization and hence the NMR signal vanishes. However, in ruby no such position has been found. Strongly polarized NMR lines and thermal equilibrium signals have an identical shape. With

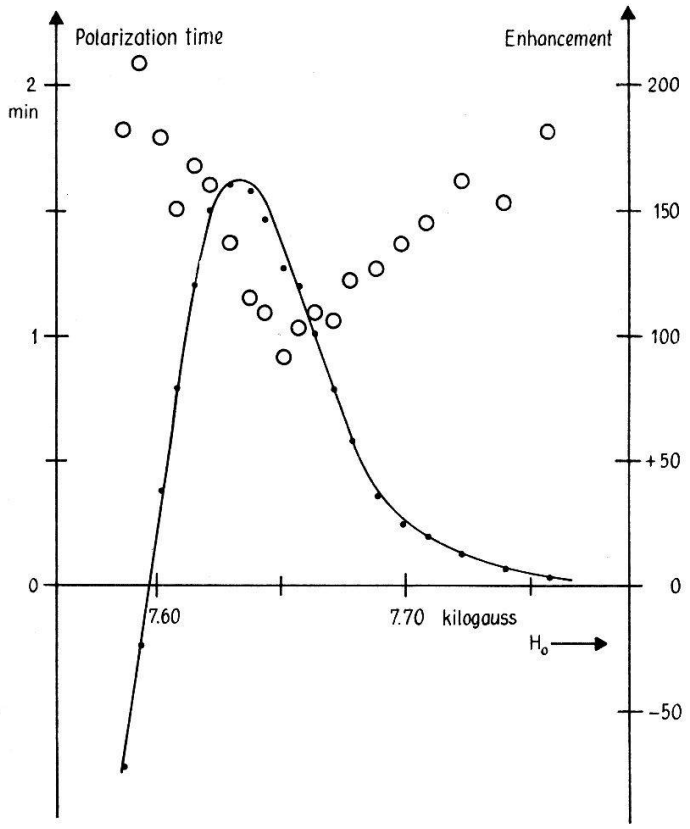

Figure 7
Polarization times (circles) and polarization curve (solid line) at 1.85 °K for 50 mW microwave power in ruby with 0.025% Cr^{3+}. The nuclear relaxation time is T_n = 1.8 min.

the microwave power supplied at the center of the ESR line unusual NMR line shapes are observed which depend on the particular ESR line being saturated and on the angle ϑ. Typical results are shown in Figure 8. The signals which arise by saturating the $-1/2 \leftrightarrow +1/2$ ESR transition (Fig. 8a) can be explained by the inhomogeneity of the magnetic field as described elsewhere [36]. The enhanced ^{27}Al NMR signals have a shape function which is proportional to the negative derivative of the thermal equilibrium shape function and the enhancement increases with the inhomogeneity of the *dc* magnetic field.

To explain the line shapes which result by saturating the $-3/2 \leftrightarrow -1/2$ ESR line (Fig. 8b) crystal imperfections have to be assumed. This line depends more strongly on the angle ϑ and the crystal field parameter D than the $-1/2 \leftrightarrow +1/2$ transition as may be seen from Figure 2. Local variations of ϑ and D thus give rise to a line broadening which affects the NMR line shape under dynamic polarization at the center of the ESR line. To illustrate a possible effect we assume for simplicity, that the crystal is made up of two domains which have a slightly different angle ϑ between their respective *c*-axes and the magnetic field. In the two domains, Cr^{3+} has a different resonance field as indicated by the solid and the dashed line in Figure 9a. Under saturation at the center of the combined line the ^{27}Al nuclei in the domain with the smaller angle ϑ will be positively polarized, while those in the domain with larger ϑ will be negatively polarized. Furthermore, slightly different quadrupole splittings result for the NMR spectra of the two domains. In first order the central line is not shifted, therefore positive and negative polarizations cancel and the line is expected to vanish. The satellites behave differently. Due to the quadrupole effects of different magnitude lines are expected which contain positively and negatively enhanced

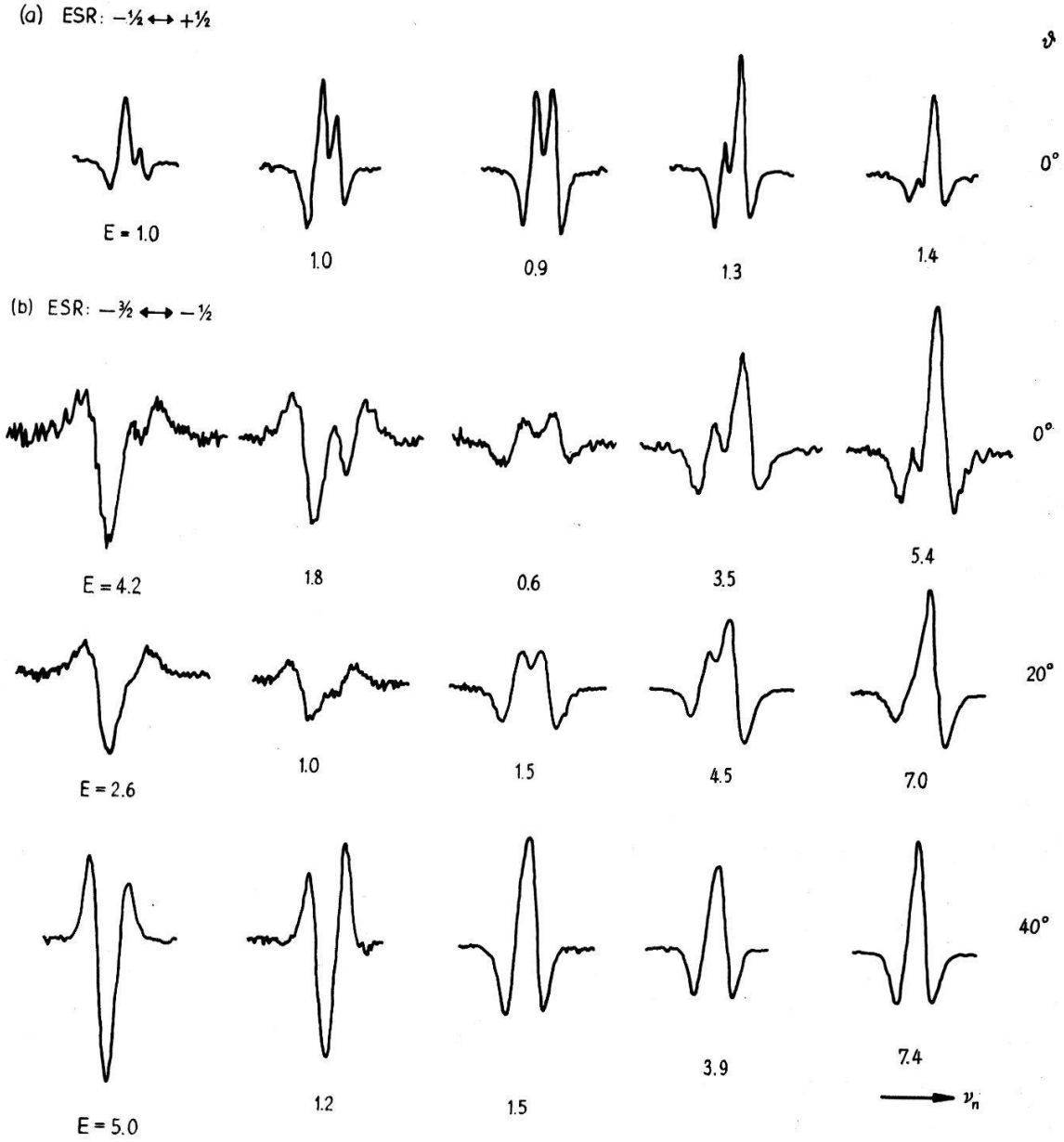

Figure 8
Derivative of the ^{27}Al NMR spectrum under irradiation of 100 mW microwave power at the center of the ESR line. $T = 4.2\,^{\circ}\mathrm{K}$, 0.025% Cr^{3+} in ruby. The modulation amplitude of the magnetic field is 1.5 gauss. E is the enhancement with respect to the corresponding thermal equilibrium signals.

portions. The resulting ^{27}Al NMR spectrum is indicated by the dotted line in Figure 9b for the case of a decreasing NMR splitting with increasing angle ϑ. The difference of the resonance frequency between positively and negatively enhanced signals is larger for the outer satellites. Thus, the outer lines have the strongest enhancements.

In a real crystal domains exist with a characteristic distribution of angles ϑ. Thus the resulting line shapes under dynamic polarization at the center of the ESR line have to be calculated from the superposition of single domain lines each properly polarized according to the ESR frequency and the angle ϑ. As in the case of a line broadening due to the inhomogeneity of the magnetic field, the NMR lines are proportional to the derivative of the thermal equilibrium signal, but two corresponding

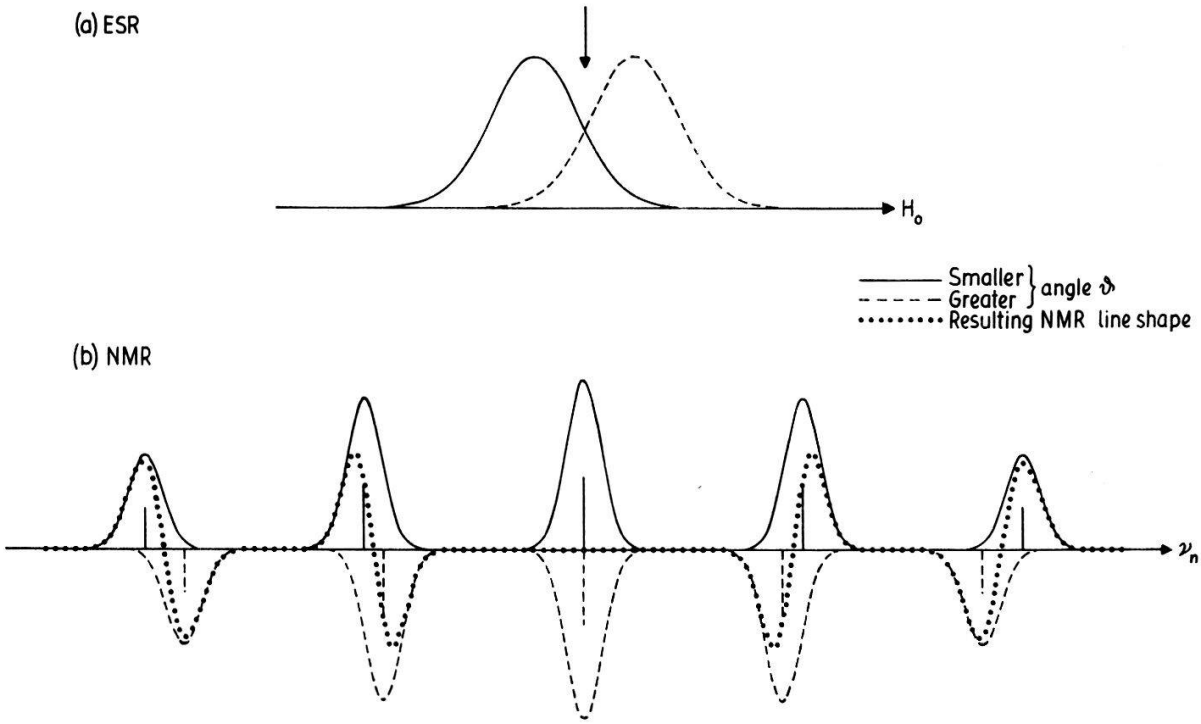

Figure 9
Model of line shape behavior in a crystal with two domains under saturation of the ESR line at its center.

satellites differ in sign. Therefore domain and magnetic field broadening effects can be discriminated. Similar calculations are in principle possible when the broadening results from a distribution of the gradients of the crystal field or from strains.

Typical ^{27}Al signals which we have observed under dynamic polarization at the center of the $-3/2 \leftrightarrow -1/2$ Cr^{3+} ESR line are given in Figure 8b. They indicate that both the inhomogeneity of the magnetic field and crystal imperfections contribute to the line shape. The nonvanishing central line arises from the field inhomogeneity present at the center of the magnet which is a small fraction of the NMR line width only. To explain the shape of the satellites both broadening mechanisms have to be assumed. In the high frequency lines both effects add, whereas in the low frequency satellites partial cancellation takes place, thus yielding a different enhancement of corresponding satellites. For increasing inhomogeneity the low frequency satellites become smaller and finally even change their sign. Furthermore, the enhancement of the outer satellites is considerably larger than that of the inner ones. The change of the line shape with the angle ϑ as shown in Figure 8b is due to a corresponding variation of the thermal equilibrium signal with ϑ. The resolved dipole structure of the ^{27}Al NMR line disappears with increasing ϑ. Qualitatively, all the observed line shapes can be explained with the simple models proposed above. Thus it has been shown that different line broadening mechanisms can be investigated with this new dynamic polarization technique. For a quantitative approach, however, more refined considerations are necessary.

In summing up, the following remarks may be added. For a homogeneously broadened ESR line the polarization should vanish when the ESR line is saturated at its center. For a line which is inhomogeneously broadened by spin-spin or other local interactions a temperature dependent effect might occur, which has been proposed

by Verber and Lecander [37] and Lee [38]. However, it has not been observed unambiguously so far. In the case, where both the ESR and the NMR lines are broadened simultaneously by means of a long range interaction, polarization effects as described above are expected. Particularly, this occurs when the line broadening is due to the inhomogeneity of the magnetic field, to a domain structure, or to crystal strains. In this case the line shapes and enhancements are independent of the temperature, if the slope of the polarization curve near its center does not depend on T. By its temperature dependence, this effect therefore can be clearly distinguished from effects, which arise from local interactions.

III. Theoretical Aspects

A complete theory of dynamic nuclear polarization which would explain our experimental results is not available presently. The spin temperature theory of dynamic polarization as developed by Borghini [4] will be used here. In order to take into account the electrical interactions of paramagnetic ions and nuclei slight modifications are made in a phenomenological manner.

Borghini's theory is based on the theories of magnetic resonance saturation in solids by Redfield [39] and Provotorov [40]. The basic assumption is the existence of three different energy reservoirs, formed by the electron Zeeman, the electron dipole, and the nuclear Zeeman system respectively, each being in thermal equilibrium. Hence a spin temperature can be assigned to each subsystem. This is thought to be true also under saturation conditions, when a strong microwave field of frequency ω is applied to the spin systems. The density matrix of the electron-nuclear system in the rotating frame of reference is assumed to be

$$\sigma^* \propto \exp[-\alpha\,(\omega_e - \omega)\,S_z - \beta\,\omega_n\,I_z - \gamma\,\mathcal{H}_{SS}^0]\,.$$

α, β and γ are the inverse temperatures of the electron Zeeman, the nuclear Zeeman, and the electron dipole reservoir. S_z and I_z are the electronic and nuclear angular momentum operators, ω_e and ω_n the corresponding Larmor frequencies. $\mathcal{H}_{SS}^0$ is the time independent part of the electronic dipole-dipole interaction energy. In the high temperature approximation, as the only one being treated, the density matrix is given by

$$\sigma^* \propto 1 - \alpha\,\Delta\,S_z - \beta\,\omega_n\,I_z - \gamma\,\mathcal{H}_{SS}^0$$

where $\Delta = \omega_e - \omega$.

The influence of the spin lattice relaxation and the microwave radiation on the inverse temperatures α, β and γ are considered separately. The relaxation variations are given by [4, 41]

$$\left(\frac{\partial\alpha}{\partial t}\right)_L = -\frac{1}{T_e}\left(\alpha - \frac{\omega_e}{\Delta}\,\beta_L\right), \tag{5}$$

$$\left(\frac{\partial\beta}{\partial t}\right)_L = -\frac{1}{T_n}\,(\beta - \beta_L)\,, \tag{6}$$

$$\left(\frac{\partial\gamma}{\partial t}\right)_L = -\frac{2}{T_e}\,(\gamma - \beta_L)\,. \tag{7}$$

Here $\beta_L = 1/k\,T$ is the inverse lattice temperature, T_e and T_n are the electronic and nuclear relaxation times. We assume that the ESR line is broadened by spin-spin interactions of the paramagnetic ions, which leads to a homogeneously broadened line. Then the rate of change due to the r.f. field is given by [4, 42]:

$$\left(\frac{\partial\alpha}{\partial t}\right)_{H_1} = -W_0\,(\alpha-\gamma) - N\,\frac{\omega_n}{\Delta}\,(W^- - W^+)\,(\alpha-\beta)\,, \tag{8}$$

$$\left(\frac{\partial\beta}{\partial t}\right)_{H_1} = -W^-\left[\beta - \frac{\Delta}{\omega_n}\,\alpha - \left(1-\frac{\Delta}{\omega_n}\right)\gamma\right] - W^+\left[\beta + \frac{\Delta}{\omega_n}\,\alpha - \left(1+\frac{\Delta}{\omega_n}\right)\gamma\right], \tag{9}$$

$$\left(\frac{\partial\gamma}{\partial t}\right)_{H_1} = -\frac{\Delta^2}{\omega_L^2}\,W_0\,(\gamma-\alpha) - N\,\frac{\omega_n^2}{\omega_L^2}\left[W^-\left(1-\frac{\Delta}{\omega_n}\right) + W^+\left(1+\frac{\Delta}{\omega_n}\right)\right](\gamma-\beta)\,. \tag{10}$$

$W_0 = W_0\,(\omega_e - \omega)$ is the ESR transition probability, $W^- = W^-\,(\Delta - \omega_n)$ and $W^+ = W^+\,(\Delta + \omega_n)$ are the probabilities of the 'forbidden' transitions, which correspond to mutual flips of one electronic and one nuclear spin. They are weaker than the allowed transitions W_0 by a factor T_e/T_n. N is the ratio of the number of nuclei and paramagnetic ions in the sample. ω_L is related to the local field H_L of the electrons and the second moment $\overline{\Delta H^2}$ of the unsaturated ESR line by the equation

$$\omega_L^2 = \gamma_e^2\,H_L^2 = \frac{1}{3}\,\gamma_e^2\,\overline{\Delta H^2}\,.$$

For the steady state solutions the total rate of change for α, β and γ must fulfill the condition

$$\frac{d}{dt} \equiv \left(\frac{\partial}{\partial t}\right)_L + \left(\frac{\partial}{\partial t}\right)_{H_1} = 0\,. \tag{11}$$

The steady state solutions for α, β and γ in the rotating frame can be calculated from equations (5) to (11). β is also the inverse nuclear spin temperature in the laboratory frame and β/β_L gives the enhancement of the nuclear polarization in this frame.

Borghini's briefly summarized theory is valid for spins greater than 1/2 only under certain conditions. Particularly for the case of ruby some modifications have to be made. In addition to the magnetic spin interactions also electric interactions are present. ^{27}Al has a nuclear spin $I = 5/2$ and a nonvanishing electric quadrupole moment. Its interaction energy with the crystal field gradient tensor [6] is less than 10% of the nuclear magnetic energy in a typical magnetic field of 10 kilogauss. The fine structure splitting of the ESR lines [5] is about 50% of the magnetic splitting for such a field. In Borghini's theory the transition frequencies ω_e and ω_n are used as a measure of the Zeeman energies. We will take into account the electric interactions by inserting into equations (5), (8), (9) and (10) the transition frequencies ω_e and ω_n,

arising from magnetic *and* electric interactions. With this assumption we treat the total spin energy like a pure magnetic one of the same magnitude.

As pointed out, the basic assumption of the spin temperature theory is the existence of defined inverse temperatures α, β and γ for the corresponding spin systems. This condition is fulfilled for the ^{27}Al nuclei also under dynamic polarization (see Chap. II.7). It is not met, however, for the Cr^{3+} spin system. In its ground state Cr^{3+} in ruby has an effective spin $S = 3/2$. Because of the fine structure splitting the ESR transitions have different frequencies. In a dynamic polarization experiment usually only one ESR line is saturated at a time and unique inverse temperatures α and γ for the electronic spin system cannot be defined. The electronic spin of a Cr^{3+} ion will be during times τ_p at resonance with the microwave field and will thus polarize the ^{27}Al nuclei. During times τ_r it is affected only by the spin lattice interactions and thereby relaxes the nuclei. During τ_r therefore the ^{27}Al polarization decreases.

β approaches its equilibrium value with a polarization time T_{np} during time intervals τ_p:

$$\left(\frac{\partial\beta}{\partial t}\right)_p = -\frac{\beta-\beta_p}{T_{np}}. \tag{12}$$

β_p can be calculated from equations (5) to (11). During τ_r the nuclear spin temperature approaches the lattice temperature:

$$\left(\frac{\partial\beta}{\partial t}\right)_r = -\frac{\beta-\beta_L}{T_n}. \tag{13}$$

Equilibrium is reached when the increase of the polarization during the averaged time τ_p equals the decrease during the averaged time τ_r [43]:

$$\tau_p \frac{\beta-\beta_p}{T_{np}} = -\tau_r \frac{\beta-\beta_L}{T_n}.$$

The inverse equilibrium temperature is then

$$\bar{\beta} = \frac{\beta_p \frac{\tau_p}{T_{np}} + \beta_L \frac{\tau_r}{T_n}}{\frac{\tau_p}{T_{np}} + \frac{\tau_r}{T_n}}.$$

Our experiments show that even for the highest microwave power available the measured polarization time T'_{np} is not much shorter than the nuclear relaxation time T_n (see Chap. II.7). Therefore also T_{np} must be of the order of magnitude of T_n. Hence we consider the approximation $T_{np} = T_n$ only. In this case the equilibrium polarization can be calculated from

$$\bar{\beta} = \frac{\beta_p \tau_p + \beta_L \tau_r}{\tau_p + \tau_r}. \tag{14}$$

It has been assumed that all paramagnetic ions have the same Larmor frequency and that the width of their resonance lines is given by the dipole-dipole interaction $\mathcal{H}_{SS}$. In the case of inhomogeneous broadening different spins have different Larmor frequencies due e.g. to lattice defects or to the interaction of the electronic spins S with neighboring nuclei. Both causes of ESR line broadening have been found in ruby [22–24]. In the case of inhomogeneous broadening the ESR line may be thought to consist of spin packets [25] having different frequencies. This does not imply, however, that they are independent from each other. When saturating one spin packet an equilibrium among the packets with a correlation time T_3 will be reached [44]. If T_3 is long compared with the electronic relaxation time T_e, the spin packets are approximately independent of each other. If T_3 is short compared with T_e, the ESR line behaves like a homogeneously broadened one and the polarization can be derived from the equations above.

For the case of an inhomogeneously broadened ESR line with independent spin packets the polarization of all nuclei which are polarized by the electrons of this packet, can be calculated from equation (14). In assuming that the packet does not change its resonance frequency in a time which is long compared with the nuclear relaxation time T_n, the average nuclear polarization can be calculated from

$$\bar{\beta} = \frac{\sum_i g_i \beta_i}{\sum_i g_i} \tag{15}$$

where g_i is the number of electrons in the i^{th} spin packet. The inverse nuclear spin temperature β_i, induced by these electrons, is again given by equation (14). If the resonance frequencies of the packets change rapidly relative to T_n, the average polarization can be calculated in analogy to equations (12), (13) and (14) from

$$\bar{\beta} = \frac{\sum_i \tau_i \beta_i}{\sum_i \tau_i} . \tag{16}$$

The time τ_i an electronic spin spends in the i^{th} spin packet is proportional to the number g_i of spins in this packet. As the time average equals the space average, we cannot distinguish with our model whether the spin packets do not change their frequencies or whether they change them rapidly compared with T_n.

In a ruby with 0.025% Cr^{3+} and $\vartheta \approx 0°$ the ^{27}Al nuclear polarization was measured as a function of magnetic field strength and microwave power. The modulation amplitude of the magnetic field was 1.5 Gauss at 4.2 °K and 77 °K, and 0.5 Gauss at 1.85°K. No marked dependence upon the modulation amplitude was found for the polarization curves.

The polarization curves as functions of the field and for a fixed frequency are computed from the theory by solving the system of linear equations (5) to (10) with condition (11). The rather cumbersome results shall not be given here. The parameters used for the calculations are:

ω_e the Cr^{3+} ESR frequency,

ω_n the ^{27}Al NMR frequency,

ΔH_G the full width of the Gaussian envelope curve of the ESR line, measured between points of maximum slope,

ΔH_L half the width at half maximum of the Lorentzian spin packets,

N the ratio of the number of nuclear and electronic spins,

T_n/T_e the ratio of nuclear and electronic relaxation times,

$W_0 T_e = A \times f(H)$ the product of ESR transition probability and electronic relaxation time where $f(H)$ is the normalized ESR line shape function calculated with ΔH_G and ΔH_L,

τ_r/τ_p the ratio of averaged times τ_r and τ_p, for which an electron spin makes relaxing transitions only, respectively for which it is in resonance with the microwave field, and

H_L the local field.

Out of these parameters only ω_e and ω_n have been measured directly. ΔH_G and ΔH_L have been determined from the measured line shape to which a shape function $f(H)$ according to equation (2) is fitted (Fig. 3). The ratio of nuclear and electronic spins was calculated from the chromium concentration as quoted by the manufacturer and is $N = 7.7 \times 10^3$ for this specimen. The last terms in equations (8) and (10) are proportional to $N \times T_e/T_n$. They arise from the conservation of the total energy,

$$\alpha \Delta^2 + N \beta \omega_n^2 + \gamma \omega_L^2 .$$

For spins $> 1/2$ the ratio of spin numbers therefore should be multiplied by the ratio of the specific heat of the spin systems. We then have for $S = 3/2$ and $I = 5/2$ in ruby with 0.025% Cr^{3+}: $N = 2.33 \times 7.7 \times 10^3 = 1.8 \times 10^4$.

Table 3
Electronic relaxation times T_e of 0.025% Cr^{3+} in ruby for $\vartheta \approx 0°$ and transitions with $\Delta m = 1$.

T	T_e
1.85 °K	50 msec
4.2 °K	20 msec
77 °K	50 μsec

The electronic relaxation time T_e has not been measured by us. Results have been reported by various authors [45–49]. We will use the values listed in Table 3 for $\Delta m = 1$ ESR transitions. At temperatures of liquid helium the relaxation time for transitions with $\Delta m = 2$ is twice as long and for $\Delta m = 3$ four times as long as T_e for $\Delta m = 1$. At 77 °K all the transitions have identical relaxation times [45, 46]. In Table 4 the nuclear relaxation times T_n are given, which have been measured in our experiments. For the theoretical polarization curves the ratio T_n/T_e is calculated from the values of T_e and T_n in Tables 3 and 4. The magnetic microwave field strength in the cavity, which contains the crystal and the NMR coil is not known. Therefore an absolute determination of A is impossible. The relative differences of A are known in experiments, however, where only the microwave power is changed by a known

amount. The absolute value of A was determined by approximation of the measured curves with theoretical ones by varying A. With the values for A evaluated in this way and with the relaxation times T_e of Table 3 the microwave field strength in the cavity is 40 milligauss for an incident power of 50 mW.

Table 4
^{27}Al nuclear relaxation times T_n in ruby with 0.025% Cr^{3+} at $\vartheta \approx 0°$.

T	T_n at $H_0 = 7.6$ kG	T_n at $H_0 = 11.7$ kG
1.85 °K	90 sec	140 sec
4.2 °K	45 sec	–
77 °K	3.5 sec	5.4 sec

The ratio τ_r/τ_p has been estimated from the Boltzmann populations of the four ESR levels. For this estimation the different relaxation times T_e for transitions with $\Delta m = 1$, 2 and 3 have also been considered. For investigating the dynamical behavior of the electrons the polarization curves have been calculated for the limits of completely dependent and independent spin packets. In the first case the measured second moment $\overline{\Delta H^2}$ of the ESR lines was used for the calculation of the local field $H_L = \sqrt{(1/3)\,\overline{\Delta H^2}}$. In the case of independent spin packets the value of the spin packet width ΔH_L was used for H_L.

Figures 10, 11 and 12 show the experimental and theoretical polarization curves. The parameters of the calculated curves are listed in Table 5. The values of A given there correspond to the respective greatest microwave powers. For the remaining curves, A was calculated from the power ratios. H_L denotes the local field for the case of dependent spin packets. In the line marked 'ESR' the transition is given, which was saturated for achieving the polarization.

In Figures 10, 11 and 12 measured points are connected by solid lines. The experimental data were taken with rubies with 0.025% Cr^{3+} at $\vartheta \approx 0°$. The dashed curves are computed for the approximation of an ESR line that behaves like a homogeneously broadened one. The curves drawn with dashes and dots show the

Table 5
Parameters of the calculated polarization curves.

Figure	10	11	12
T	1.85	77	77 °K
ESR	$-3/2 \leftrightarrow -1/2$	$-3/2 \leftrightarrow -1/2$	$-1/2 \leftrightarrow +1/2$
$\omega_e/2\pi$	32.45	33.10	33.10 GHz
$\omega_n/2\pi$	8.43	8.65	13.23 MHz
ΔH_G	15.40	15.40	10.13 gauss
ΔH_L	4.82	4.82	3.39 gauss
T_n/T_e	1800	$7 \cdot 10^4$	$1.08 \cdot 10^5$
A	2000	20	20 gauss
τ_r/τ_p	0.5	5.0	5.0
H_L	7.95	7.95	7.54 gauss

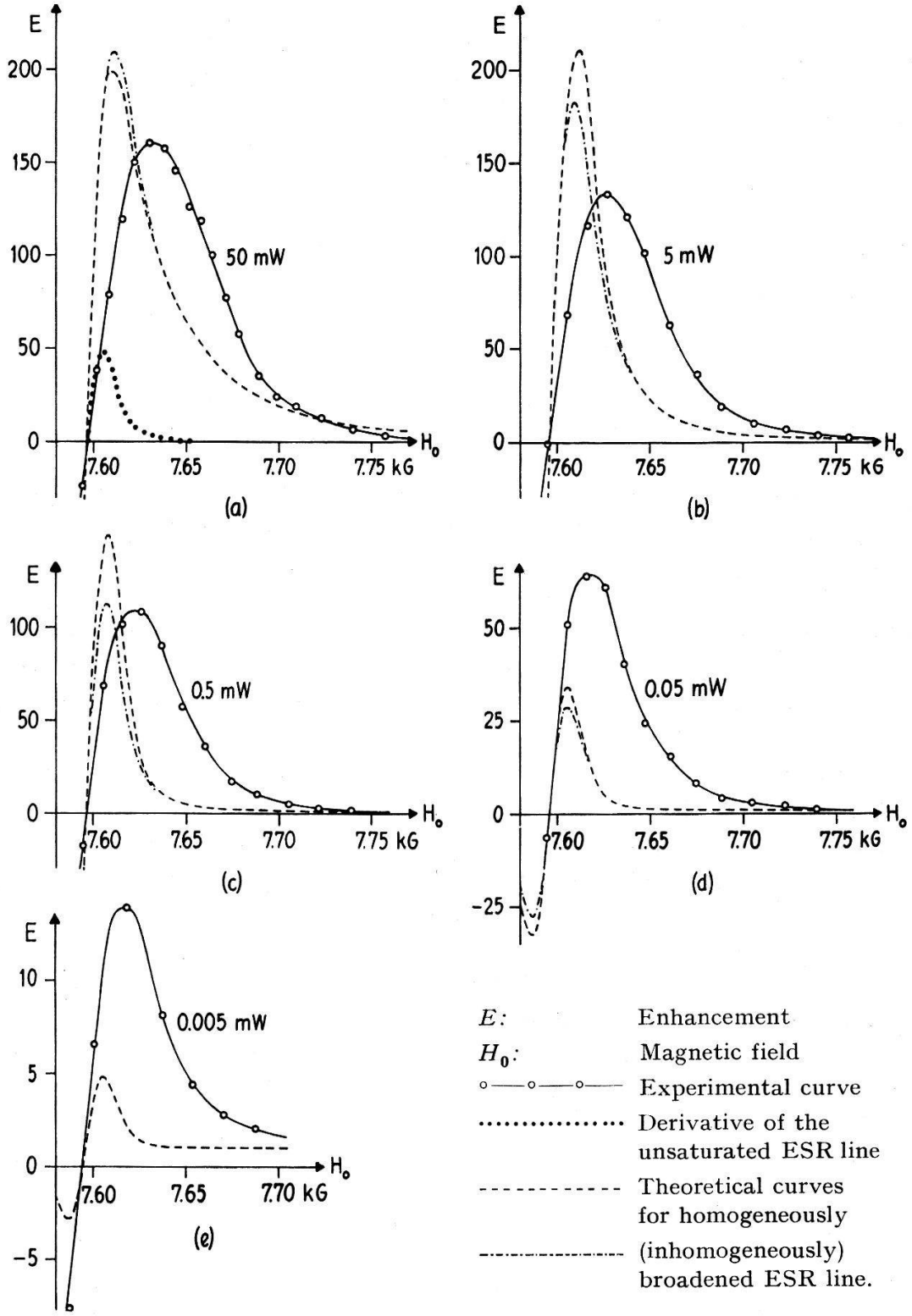

Figure 10
Polarization curves at 1.85 °K under saturation of the $-3/2 \leftrightarrow -1/2$ ESR transition.

theoretical polarization curves for the approximation of completely independent spin packets. In Figures 10a, 11a and 12a also the derivative of the ESR line is given by a dotted line. The curves in Figures 11 and 12 have been taken at 77 °K under exactly the same conditions. The microwave power given there cannot be compared directly

with those of Figure 10, because the resonance frequency and the Q-value of the cavity change with temperature.

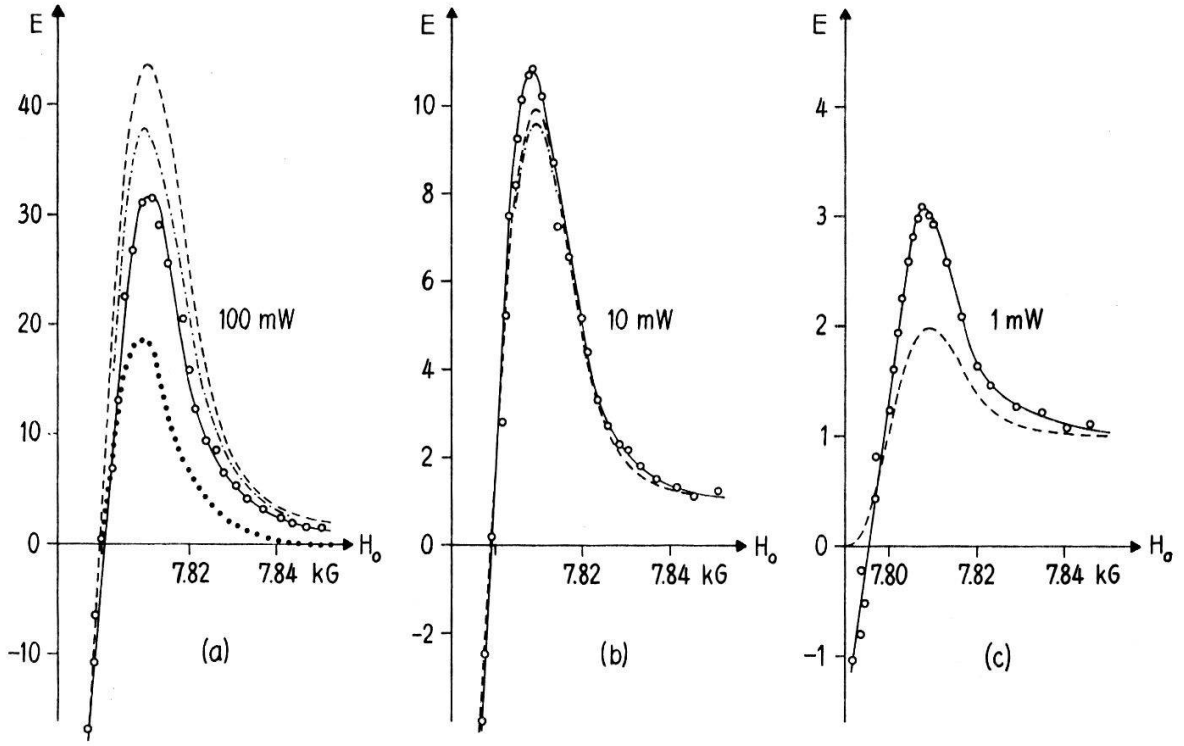

Figure 11
Polarization curves at 77 °K under saturation of the $-3/2 \leftrightarrow -1/2$ ESR transition.

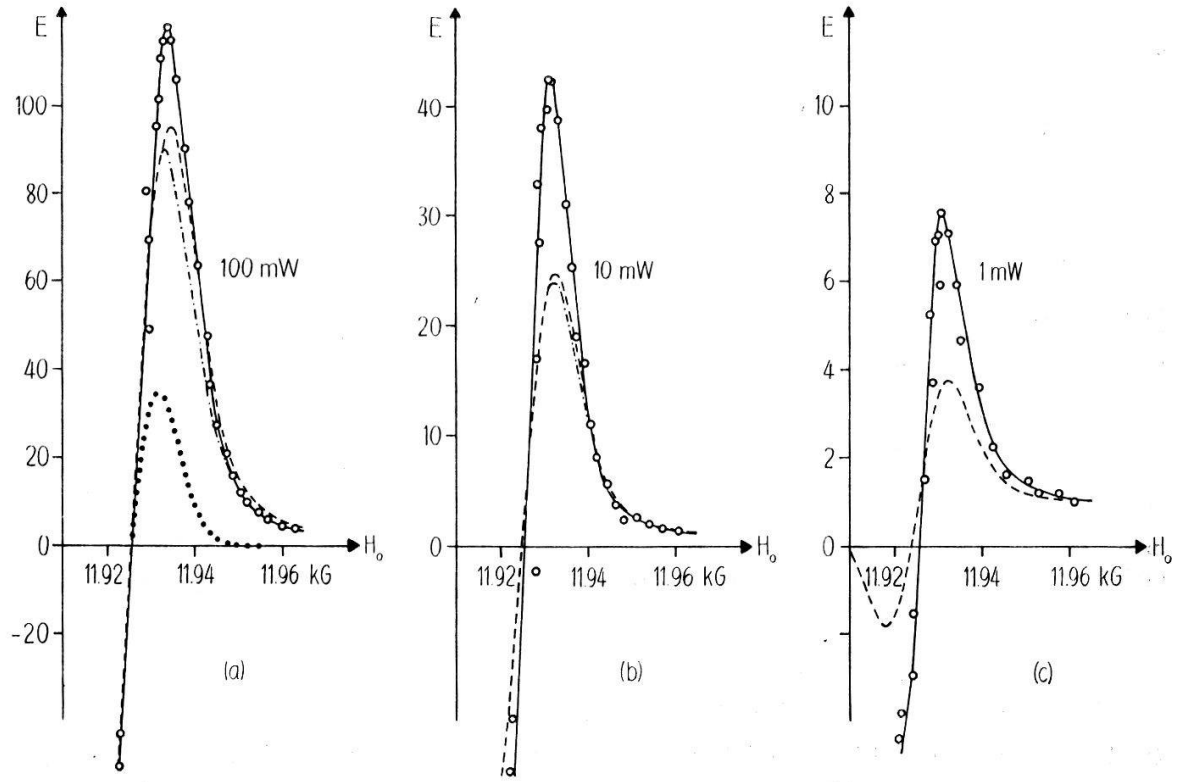

Figure 12
Polarization curves at 77 °K under saturation of the $-1/2 \leftrightarrow +1/2$ ESR transition.

At 77 °K a greater enhancement is reached when the $-1/2 \leftrightarrow +1/2$ ESR line is saturated instead of the $-3/2 \leftrightarrow -1/2$ transition due to the smaller width of the $-1/2 \leftrightarrow +1/2$ line. At 1.85 °K the enhancement is only 33 for this line and 160 for the $-3/2 \leftrightarrow -1/2$ transition. This can be explained by the fact that τ_r/τ_p at 77 °K has about the same value for all transitions. At the temperature of liquid helium, however, it is smaller for the $-3/2 \leftrightarrow -1/2$ transition than for the $-1/2 \leftrightarrow +1/2$ transition because of the lower populations of the higher ESR levels.

The agreement between experiment and theory is at least qualitatively good at 77 °K. Particularly, the width of the polarization curves is predicted correctly by the theory. At the temperature of liquid helium an essentially greater width is found which cannot be explained by Borghini's theory. Also, when the parameters listed in Table 5 are varied within wide limits, no better agreement between theory and experiment can be reached. In lanthanum magnesium nitrate at helium temperature too great a width was also found [42]. This was explained partly by a phonon bottleneck in the elctron spin relaxation. Such a bottleneck can be excluded for the relaxation of the Cr^{3+} ground state in ruby [50, 51]. The reason for the disagreement between theory and experiment is not yet understood. A possible cause might be the application of the high temperature approximation at the temperature of liquid helium. Because of this disagreement no distinction is possible, whether the ESR line behaves under dynamic polarization conditions like a homogeneously broadened one, or whether the spin packets are really independent, or whether the real situation lies between these two extreme cases.

Acknowledgements

We would like to express our gratitude to Professor O. S. Leifson, who initiated the dynamic nuclear polarization research in our laboratory and who constructed parts of our experimental setup. We are indebted to the Industrie de Pierres Scientifiques Hrand Djévahirdjian S.A., Monthey, Switzerland, for donating the Verneuil-grown crystals.

REFERENCES

[1] A. Abragam, Phys. Rev. *98*, 1729 (1955).
[2] A. Abragam, W. G. Proctor, C.R. Acad. Sci. *246*, 2253 (1958).
[3] O. S. Leifson, C. D. Jeffries, Phys. Rev. *122*, 1781 (1961).
[4] A. Abragam, M. Borghini, Progr. in Low Temp. Phys. Vol. IV (North-Holland, Amsterdam 1964), p. 384.
[5] E. O. Schulz-du Bois, Bell Syst. Tech. J. *38*, 271 (1959).
[6] R. V. Pound, Phys. Rev. *79*, 685 (1950).
[7] R. W. Terhune, J. Lambe, G. Makhov, L. G. Cross, Phys. Rev. Lett. *4*, 234 (1960).
[8] J. Lambe, N. Laurance, E. C. McIrvine, R. W. Terhune, Phys. Rev. *122*, 1161 (1961).
[9] R. W. Terhune, J. Lambe, C. Kikuchi, J. Baker, Phys. Rev. *123*, 1265 (1961).
[10] N. Laurance, E. C. McIrvine, J. Lambe, J. Phys. Chem. Solids *23*, 515 (1962).
[11] Yu. V. Vladimirtsev, V. A. Golenishchev-Kutuzov, U. Kh. Kopvillem, N. A. Shamukov, JETP Letters *9*, 49 (1969).
[12] H. H. Niebuhr, thesis, Universität Zürich, 1969.
[13] G. M. Zverev, A. M. Prokhorov, Sov. Phys. JETP *7*, 707 (1958).
[14] L. S. Kornienko, A. M. Prokhorov, Sov. Phys. JETP *11*, 1189 (1960).

[15] S. A. Marshall, A. R. Reinberg, J. appl. Phys. *31* (Suppl.), 336 S (1960).
[16] V. M. Vinokurov, M. M. Zaripov, N. R. Yafaev, Sov. Phys. JETP *10*, 220 (1960).
[17] S. Geschwind, J. P. Remeika, Phys. Rev. *122*, 757 (1961).
[18] G. M. Zverev, A. M. Prokhorov, Sov. Phys. JETP *12*, 41 (1961).
[19] J. C. Gill, Nature *190*, 619 (1961).
[20] L. Rimai, H. Statz, M. J. Weber, G. A. deMars, G. F. Koster, Phys. Rev. Lett. *4*, 125 (1960).
[21] C. A. Bates, J. M. Dixon, J. Phys. C (Solid St. Phys.), Ser. 2, *2*, 2225 (1969).
[22] W. J. C. Grant, M. W. P. Strandberg, Phys. Rev. *135*, A 727 (1964).
[23] R. F. Wenzel, Y. W. Kim, Phys. Rev. *140*, A 1592 (1965).
[24] C. J. Kirkby, J. S. Thorp, J. Phys. C (Proc. Phys. Soc.), Ser. 2, *1*, 913 (1968).
[25] A. M. Portis, Phys. Rev. *91*, 1071 (1953).
[26] M. H. Cohen, F. Reif, Solid St. Phys., Vol. *5* (Academic Press, New York 1957), p. 321.
[27] A. H. Silver, T. Kushida, J. Lambe, Phys. Rev. *125*, 1147 (1962).
[28] J. A. Cowen, W. R. Schafer, R. D. Spence, Phys. Rev. Lett. *3*, 13 (1959).
[29] R. D. Spence, J. A. Cowen, J. Chem. Phys. *32*, 624 (1960).
[30] R. K. Jeck, V. P. Jacobsmeyer, S. Lee, Bull. Am. Phys. Soc. *10*, 1119 (1965).
[31] A. Abragam, *The Principles of Nuclear Magnetism* (Clarendon Press, Oxford 1961), p. 261.
[32] A. Abragam, M. Chapellier, Phys. Lett. *11*, 207 (1964).
[33] D. Strominger, J. M. Hollander, G. T. Seaborg, Rev. Mod. Phys. *30*, 585 (1958).
[34] E. Brun, E. Hundt, H. Niebuhr, Helv. phys. Acta *41*, 417 (1968).
[35] V. A. Atsarkin, M. I. Rodak, Sov. Phys. Solid State *11*, No. 3, 493 (1969).
[36] H. H. Niebuhr, E. E. Hundt, E. Brun, Phys. Rev. Lett. *21*, 1735 (1968) and *22*, 159 (1969).
[37] C. M. Verber, R. G. Lecander, Phys. Lett. *25A*, 179 (1967).
[38] S. Lee, Phys. Lett. *26A*, 572 (1968).
[39] A. G. Redfield, Phys. Rev. *98*, 1787 (1955).
[40] B. N. Provotorov, Sov. Phys. JETP *14*, 1126 (1962).
[41] N. Bloembergen, E. M. Purcell, R. V. Pound, Phys. Rev. *73*, 679 (1948).
[42] T. J. B. Swanenburg, G. M. van den Heuvel, N. J. Poulis, Physica *33*, 707 (1967).
[43] P. Zegers, R. van Steenwinkel, Physica *33*, 332 (1967).
[44] S. Clough, C. A. Scott, J. Phys. C (Proc. Phys. Soc.), Ser. 2, *1*, 919 (1968).
[45] J. H. Pace, D. F. Sampson, J. S. Thorp, Phys. Rev. Lett. *4*, 18 (1960).
[46] J. H. Pace, D. F. Sampson, J. S. Thorp, Proc. Phys. Soc. *76*, 697 (1960).
[47] K. J. Standley, R. A. Vaughan, Phys. Rev. *139*, A 1275 (1965).
[48] R. A. Lees, W. S. Moore, K. J. Standley, Proc. Phys. Soc. *91*, 105 (1967).
[49] D. R. Mason, J. S. Thorp, Phys. Rev. *157*, 191 (1967).
[50] N. S. Shiren, E. B. Tucker, Phys. Rev. Lett. *2*, 206 (1959).
[51] C. Kikuchi, J. Lambe, G. Makhov, R. W. Terhune, J. appl. Phys. *30*, 1061 (1959).